Instrumentation for photocrystallographic experiments of transient species

Wilfred K. Fullagar, Guang Wu, Chris Kim, Lynn Ribaud, Gary Sagerman and Philip Coppens*

Department of Chemistry, State University of New York at Buffalo, Buffalo, NY 14260-3000, USA. E-mail: coppens@acsu.buffalo.edu

Instrumentation for stroboscopic time-resolved diffraction studies at low temperatures is described. Exciting laser light is delivered to the crystal through an optical fiber. During the diffraction experiment, fluorescence from the sample is focused onto a fiber optic bundle surrounding the laser-light fiber, and monitored by a photodiode. A rotating slotted disk produces a pulsed X-ray beam with pulse frequencies suitable for the study of molecular excited states with lifetimes of 10 μs or longer. Synchronization of the laser-pump/X-ray-probe pulses is achieved through a trigger signal from a photosensor mounted on the rotating disk, or from an X-ray sensitive photodiode inserted in the beamstop. For the study of shorter-lived species the time structure of the synchrotron beam is to be used. Equations are derived for the maximum and average fractional excited-state populations as a function of lifetime, pulse frequency and the fraction of molecules being excited by the laser pulse.

Keywords: time-resolved experiments; excited states; fractional excited-state populations; fluorescence measurements.

1. Introduction

Though X-ray crystallography has traditionally been used for the study of ground-state structure, recent technical advances are such that this limitation can now be removed (Coppens, 1997). With this in mind, several years ago we initiated studies on photoinduced metastable transition-metal nitrosyl complexes, with the long-range goal to determine the geometry and eventually the electron density of short-lived transient species (Coppens *et al.*, 1998). The success of recent time-resolved studies of reactions in proteins (Ren *et al.*, 1996; Bourgeois *et al.*, 1996; Genick *et al.*, 1997; Srajer *et al.*, 1996; Moffat, 1998) provides further impetus for the study of transient species of chemical interest.

We describe here equipment for time-resolved experiments in which the brightness of third-generation synchrotron sources is to be combined with helium-temperature cooling equipment, high-power pulsed laser light guided by optical fibers, and parallel X-ray data-collection techniques. Excitation is initiated by a laser pulse, which is followed by a probing X-ray pulse. For reversible processes the pump and probe cycle can be repeated in a stroboscopic experiment in order to obtain adequate intensity statistics for each recorded frame. As the experiments aim at ultimate resolution at the atomic level or better, monochromatic methods rather than the Laue technique will be used. The brightness of the third-generation sources will allow minimization of the exposure time, which is crucial for crystals suffering laser-radiation damage.

2. Experimental arrangement

A high-power pulsed laser is used as the periodic excitation source. Currently our system includes a diode-pumped pulsed Nd-YAG laser, operable in either CW or pulsed mode, capable of pulse rates in excess of 5 kHz and energies of up to 300 μJ per pulse at 355 nm. Pulse widths are typically ∼100 ns. While the 355 nm radiation allows study of a series of systems, a tuned laser system will eventually be installed to allow selection of a specific absorption band.

To probe a short-lived species soon after the excitation occurs, a pulsed X-ray source is required. For fast processes with lifetimes in the sub-ns to μs range, individual synchrotron beam pulses can be used. For the study of longer-lived states with lifetimes in the 10 μs to ms range, such as triplet states of chemical interest, better use is made of the X-ray beam by selection of a train of X-ray pulses, of length adjusted to the lifetime of the system being studied. In this way the average X-ray beam intensity is not excessively compromised.

To measure the diffraction pattern soon after excitation, either a very fast periodic shutter or a detector with very fast readout is needed. A scintillation detector can be gated, but as such detectors can only examine a single point in reciprocal space at any one time, very long data-collec-

tion times are required. An image plate or CCD detector cannot be gated, but will allow analysis of a small volume of reciprocal space on any one frame, thus greatly accelerating the rate of data collection. A very fast readout area detector would obviously be extremely useful, provided accuracy of measurement is not sacrificed. An imaging microstrip gas chamber with such characteristics is now under development (Tanimori *et al.*, 1996; Uekusa *et al.*, 1999). Without such a detector, a very fast shutter must be inserted into the X-ray beam to eliminate intensity measurement during the dark periods between laser pulses.

The experimental setup is illustrated in Fig. 1. Its components are (*a*) a fast periodic shutter placed behind a Bruker rotary shutter, (*b*) a pulsed laser, (*c*) a circuit for synchronizing the X-ray pulses from the shutter with the Nd-YAG laser, (*d*) a fiber-optical system for delivering the laser light to the crystal and collection of the fluorescent light emanating from the crystal onto a fluorescence detector, (*e*) a pin diode containing a beamstop for monitoring the X-ray pulses, (*f*) an optical sensor on the shutter wheel for timing purposes, and (*g*) an He gas flow system for crystal cooling and heat dissipation. The data are collected with a Bruker-CCD area detector.

More detail is given in the following sections.

3. The fast shutter

For reasons of overall simplicity, we choose a slotted wheel to chop the monochromated synchrotron beam. The wheel is mounted directly on the axle of a small electric motor, which is capable of spinning at speeds up to 20 000 r.p.m. The wheel consists of a steel or brass disk of sufficient thickness to stop the X-rays, with a diameter of 14 cm. It is easily replaced, so that the configuration of the slots can be matched to the lifetime of the species being studied. Two different designs of the wheel have been tested. The first, with 32 0.8 mm-wide radial slots gives, with 12 000 r.p.m., a beam-chopping frequency of 6400 Hz, which is somew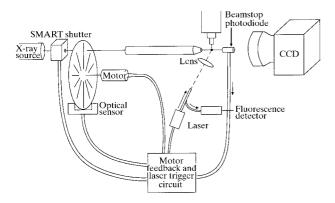hat greater than the ~5000 Hz frequency at which the T80 Nd-YAG laser delivers maximal total power. By varying the distance between the axis and the synchrotron beam, the duty cycle of the chopped radiation with this disk can be varied continuously from ~6.7% to ~10.8%. The second wheel, illustrated in Fig. 2, is to be used for much longer lifetime species. At equally spaced positions along the circumference of the wheel, eight segments of 22.5, 11.25, 4.5 and 2.25° have been removed, leading to fixed duty cycles of 50, 25, 10 and 5%, respectively.

Even for the narrow slots of the first disk, the sample crystal dimension (40–80 µm) is much smaller than the slot width (850 µm), so that the time profile of the X-ray intensity impinging on the crystal will be trapezoidal with a flat top for about 80% of the time. The wheel is not locked to the synchrotron ring frequency so that, for the many events occurring within even a few seconds of exposure, there will *on average* be no time structure within the trapezoidal pulse arising from the pulsed nature of the synchrotron source.

4. The laser

For short-lived species, the number of photons produced by a steady-state CW laser is inadequate for producing a conversion percentage in the crystal that is suitable for diffraction studies. Pulsed lasers, on the other hand, are capable of producing instantaneously highly intense radiation. In order to reach a conversion percentage adequate for the excited-state studies, the number of photons in the exciting laser pulse must be comparable with the number of photoactive molecules in the crystal. This is well within reach of current technology. The T80-YHP70-335Q Q-switched fiber-coupled Nd-YAG laser, currently incorporated in the system, is capable of producing a 200–400 mJ pulse energy at 5 kHz and 355 nm. This corresponds to more than 10^{14} photons per pulse. A 40 µm^3 crystal

Figure 1
Schematic diagram of the experimental arrangement for the time-resolved diffraction studies.
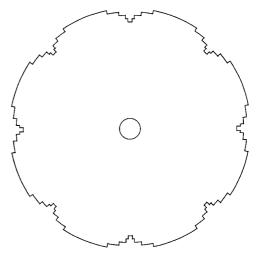

Figure 2
Drawing of one of the shutter wheels for time-resolved X-ray studies. Segments of 22.5, 11.25, 4.5 and 2.25° have been cut to provide different X-ray pulse lengths.

contains 9×10^{13} molecules with a typical molecular volume of ~ 700 Å^3. Furthermore, the photoactive molecules may be diluted by co-crystallization with inert 'spacer' molecules. We have prepared several such mixed crystalline complexes (see, for example, Zhang *et al.*, 1999).

5. Population of the excited species

The minimum excited-state population that can still be detected in the diffraction experiment depends on the experimental strategy and the nature of the photoinduced changes. Previous work indicates that very small percentages of the order of 1% or less are detectable when differences between the 'light' and 'dark' diffraction patterns are analyzed (Ozawa *et al.*, 1998). With other methods, applied in photocrystallographic studies of transition-metal nitrosyl and dinitrogen compounds, a sensitivity of several percent can be reached (Coppens *et al.*, 1998; Fomitchev *et al.*, 2000). For the determination of excited-state electron densities, much larger conversion percentages will be required.

The sequence of events and the variable excited-state population in a stroboscopic experiment as a function of time is depicted schematically in Fig. 3. We will use the following definitions in the quantitative analysis of the excited-state population as a function of time:

N_p: the number of photons per pulse;

N_{org}: the number of photoactive molecules in the crystal at the onset of the irradiation;

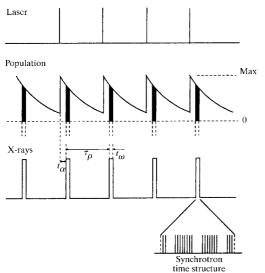N_i: the number of excited molecules just after the *i*th laser pulse;

Figure 3
Schematic diagram of the timing of the exciting laser pulse, the population of the transient species and the probing X-ray pulse in a stroboscopic time-resolved diffraction experiment. In the arrangement the synchrotron is used as a continuous source. In faster studies the time structure of the source is to be used.

N_{max}: the maximum number of excited molecules after a large number of successive pulses;

N_{min}: the number of excited molecules just before the next pulse after a large number of successive pulses;

$f(t)$: the time-dependent fractional excited-state population;

$\langle f \rangle$: the fractional excited-state population averaged over a time period;

f_{max}: the maximum fractional excited-state population pulse after a large number of successive pulses ($= N_{\text{max}}/N_{\text{org}}$);

e: the conversion efficiency, including the effect of the efficiency of focusing the laser beam on the crystal, the percentage of the photons absorbed in the crystal, and the quantum efficiency of the excitation process;

r: the fraction of ground-state molecules in the crystal being excited by the laser pulse, which is a function of e and N_p;

τ: the lifetime of the excited species;

Γ: the period between successive laser pulses, which is identical to the period between X-ray pulses;

ν_P: the pulse frequency ($= 1/\Gamma$);

t_x: the time width of the X-ray pulse;

D: the X-ray duty cycle ($= t_x/\Gamma$);

t_d: pulse to probe interval.

5.1. *Reaching of a pseudo steady state*

During each period between pulses the fraction of excited molecules decays according to

$$f(t) = f(0) \exp(-t/\tau), \tag{1}$$

where $f(0)$ is the population immediately following the laser pulse.

When $\Gamma \gg \tau$, the excited-state molecules will essentially all decay in the interval between laser pulses. However, for longer lifetimes and/or high pulse frequencies this is not the case, and cumulative pumping occurs. After an initial build-up period, a pseudo steady state is reached, in which N_{max} and N_{min}, the populations just after and just before the laser pulse, have reached constant values. This can be seen in the following.

For the first event,

$$N_1 = rN_{\text{org}}, \tag{2}$$

(thus, just after the initial pulse, $f = r$). For the following pulses,

$$N_2 = r[N_{\text{org}} - N_1 \exp(-\Gamma/\tau)] + N_1 \exp(-\Gamma/\tau), \tag{3}$$

$$N_3 = r[N_{\text{org}} - N_2 \exp(-\Gamma/\tau)] + N_2 \exp(-\Gamma/\tau), \tag{4}$$

$$N_n = rN_{\text{org}} + (1 - r)N_{n-1} \exp(-\Gamma/\tau), \tag{5}$$

which shows that the excited-state fraction immediately after pulse n is a function of r and of the ratio Γ/τ. The

graphs for a number of values of this ratio (Fig. 4) show the build-up towards and the establishment of the pseudo steady state at which the number of excited-state molecules after the pulse N_{max} has reached a plateau. For small values of the ratio Γ/τ the cumulative pumping leads to a considerable increase of the excited-state population compared with that attained immediately after the first pulse.

N_{max}, the concentration immediately after the laser pulse in the pseudo steady state, can be calculated as follows.

From (5), with $\Gamma = 1/\nu_P$,

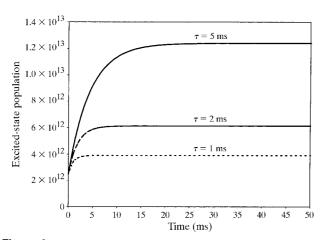$$N_{max} = rN_{org} + (1-r)N_{max}\exp[-1/(\tau\nu_p)], \qquad (6)$$

Figure 4
Build up of N_{max} as a function of time (ms). 1000 Hz laser operation and 200 mJ per pulse. From bottom to top, $\tau = 1$ ms, 2 ms and 5 ms. The total number of molecules in the crystal is 10^{14}. The excitation efficiency r is taken as 1/40. The saturation concentrations correspond to $\sim$4, 6 and 12% of the total photoactive species in the crystal [equation (5)].
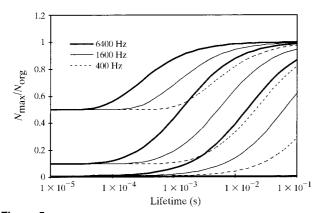

Figure 5
Ratio of excited-state population immediately after a laser pulse to the number of photoactive molecules in the sample (N_{max}/N_{org}) as a function of the lifetime τ of the excited species, for different excitation efficiencies r and different laser pulse frequencies ν_p. Values for $r = 0.01$, $r = 0.1$ and $r = 0.5$ are plotted [equation (7)].

$$N_{max}/N_{org} = r/\{1 - (1-r)\exp[-1/(\tau\nu_p)]\}. \qquad (7)$$

The results are plotted in Fig. 5.

As an example of the use of Fig. 5, we take an excited-state species with $\tau = 1$ ms and $r = 0.1$ (*i.e.* 10% of the remaining ground-state molecules are excited), and a pulse frequency of the laser and X-rays of 6400 Hz. Using these parameters and Fig. 5, the fraction f becomes $\sim$0.43, as opposed to $\sim$0.11 when the pulse frequency is 400 Hz. Both values are above the expected detection limit of the excited-state species.

In the above example the ratio N_{min}/N_{max} would be $\sim$86, so that the excited-state population is *always* very high (as one would expect for a situation in which $\tau = 6.4$ times the pulse interval), thus approaching the steady-state conditions. In that case there would be little reason to use the rotating shutter. Indeed, from the point of view of steady heat dissipation from the crystal and a steady excited-state population, one would probably be better off exciting the crystal using a CW laser of comparable (average) power.

The duration of the X-ray pulses must be selected such that the X-rays probe the system when the population of the excited state is sufficiently high to cause measurable changes to the diffraction pattern. If the X-ray pulse width is too small at a given pulse frequency, the duty cycle D will be small and the counting statistics will suffer. If the duty cycle is maintained and t_x is kept small, the pulse frequency must be increased, with the concomitant risk of burning the crystal. If the X-ray pulse width is large relative to the lifetime of the excited species, the excited-state population will vary significantly during the probe period, and the average excited-state fraction $\langle f \rangle$ will decline. The fractional population averaged over the duration of the interrogating X-ray pulse, assuming the pulse to have a square shape, is given by

$$\langle f \rangle = \frac{\int_{t_d}^{t=t_d+t_x} f(t)\exp(-t/\tau)\,dt}{\int_{t_d}^{t_d+t_x} dt} = \frac{f(t_d)\tau}{t_x}[1 - \exp(-t_x/\tau)],$$

$$(8)$$

in which $f(t_d) = f_{max}\exp(-t_d/\tau)$ accounts for the loss in excited-state population during the delay period.

Fig. 6 shows that, for $\tau \gg t_x$ (or equivalently $\tau\nu_P/D \gg 1$), the average probed population will always be close to the maximum, as there is insufficient time between pulses for the population to decay. When τ is smaller than t_x, one can pulse more rapidly, potentially destroying the crystal, or reduce t_x at the expense of the X-ray duty cycle D, otherwise the average excited-state population will be seriously compromised.

6. The optical system: guidance of the laser light and fluorescence detection

The laser light is guided through a tapered optical fiber and delivered to the crystal through a lens (fused silica lens, CVI Laser, with broad-band antireflective coating in order to optimize UV and blue-visible transmission). The arrangement avoids physical contact between the delivery system and the sample crystal, and allows focusing of the light onto the crystal. The output laser beam has a diameter of ~300 μm, which is reduced to a focal spot of diameter ~50 μm. Part of this reduction is achieved by using a tapered fiber, with input and output end core diameters of 500 μm and 100 μm, respectively. A diameter of 100 μm was selected to avoid an excessive power density and thus radiation damage from the 355 nm 0.3 mJ laser pulses. The tapered fiber acts as a numerical aperture (NA) transformer. At its narrow output end the beam divergence is increased by the ratio of the core sizes at the two ends of the fiber. The divergence α (Fig. 7) of the beam at the output end (NA = $\sin \alpha$ = 0.125 for our fiber) governs the size and distance of the lens.

The lens should intercept all the exciting light. If it is too large, the diffracted X-rays will be obstructed. If it is too close to the crystal, it will interfere with the flow of cryogen to the crystal and with the nozzle of the gas flow system. In our system a 19 mm-diameter 25 mm-focal-length lens is positioned at 70 mm from the fiber and 35 mm from the crystal, giving a focal area of diameter ~50 μm at the crystal position.

The lens fulfills a dual function. Fluorescence from the crystal is collected by the lens and refracted back towards the fiber. However, because the emitted fluorescence has a longer wavelength than the exciting light, it is refracted somewhat less, and forms an image on the fiber side of the 100 μm fiber exit window. The distance between the fiber exit window and this fluorescence image is plotted in Fig. 8. For wavelengths of interest, the excess distance is typically 3–10 mm. The light is intercepted by a 2 mm-diameter bundle of fibers surrounding the central fiber, and transmitted to a Hamamatsu photosensor module. The fiber assembly was custom-made by Fiberguide Industries.

The efficiency of the fluorescence collection is determined largely by the solid angle occupied by the lens around the crystal. The fraction of the total sphere accepted by the lens is

$$\varphi = (1 - \cos \beta)/2, \qquad (9)$$

where β is the angle subtended by the lens axis and the lens radius (Fig. 7). $\varphi \simeq 0.0175$ for the current arrangement. The fibers in the bundle occupy about 60% of the cross-sectional area of the bundle. There is a small additional loss of a few percent, owing to reflection and absorption by the lens and fiber. Before reaching the photosensor module, the light is passed through a longpass filter (400 nm edge, CVI Laser) to eliminate stray light with wavelengths less than 400 nm. The filter has ~60% transmission for fluorescence wavelengths greater than 400 nm. The combined effect of the intensity losses reduces the fraction of the light emitted by the crystal that reaches the detector to as little as 0.5%. However, in our experience it is adequate for monitoring lifetimes of the photoactive species.

7. The beamstop photodiode

A photodiode mounted in the beamstop position is used to provide X-ray timing as well as beam intensity information. The photodiode has a 3 mm² active area, 250 μm sensitive depth, an overall diameter of 3 mm, and is covered by a
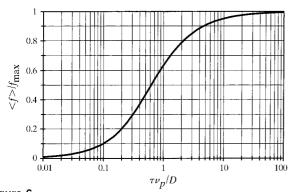

Figure 6
Ratio of excited-state population averaged over the X-ray pulse to the excited-state population immediately after the X-ray pulse, as a function of the ratio $\tau v_p/D$ (= τ/t_x) [equation (8)].
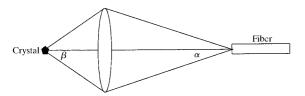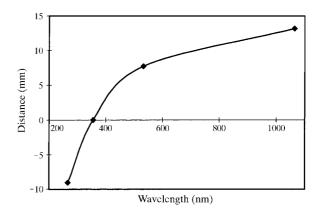

Figure 7
Schematic diagram of the light-focusing arrangement and definition of the angles α and β.

Figure 8
Distance between the exit surface of the optical fiber and the focal position of the returning fluorescent light behind the surface, as a function of the wavelength of the emitted light.

0.5 μm aluminium window which blocks visible light. Although designed for the measurement of intense X-ray bursts with energies of 1–100 keV, when reverse-biased at 200 V (photocurrent mode) it provides adequate response times for our purposes when used in the unbiased (photovoltaic) mode, without the complications of dark current. A home-built preamplifier module is used to buffer the output signal before it is sent to a comparator for the timing signal, or to other modules which convert the photodiode current into a frequency for the intensity information.

8. The synchronization circuit

The laser pulse of $\sim10^{-7}$ s duration is assumed to have a delta-function shape for the present purposes. The length of the probing X-ray pulses depends on the lifetime of the species to be studied, and can be varied by changing the slot used, the disk, or the speed of rotation of the disk.

The laser pulse must occur in exact synchronization with the excitation pulses, with a variable delay between pump and probe pulses in case geometry changes during a decay process are to be studied. This may be accomplished by phase-locking techniques. The synchronization signal can be provided either by the photodiode installed in the beamstop, or by an optical sensor mounted on the slotted disk. During periods in which the SMART shutter is closed, only the latter is available.

We have devised two different schemes. The first is relatively simple, while the second procedure allows much more accurate variation in the experimental parameters.

Scheme A. The laser is triggered by a signal taken from the photosensor on the slotted disk. It is synchronized with the X-ray signal from the beamstop photodiode by carefully adjusting the position of the wheel sensor along the disk perimeter. The delay can be adjusted by repositioning the wheel sensor. The signal from the SMART shutter is used to turn off the laser during readout or repositioning periods when the X-ray source is not probing the sample.

Scheme B. In this scheme the periodic signal is coming from either the beamstop photodiode or the optical sensor on the rotating disk, the choice of input signal being governed by whether or not the SMART shutter is opened or closed. As the beamstop photodiode signal gives more accurate X-ray timing information, it is used whenever the shutter is open.

The synchronization circuit is illustrated in Fig. 9. In order to provide an arbitrary fixed phase relationship between the pump and probe pulses, a phase-lock loop is used to generate a frequency which is 256 times the X-ray pulse frequency, thus dividing the X-ray period Γ into 256 equal sub-intervals. The laser is fired $256 - N$ pulses before the leading edge of the X-ray signal, where N can be selected by the user ($N = 0$–255). The phase-lock loop circuit incorporates a user adjustable delay variable from approximately 100 ns to about 10 μs. Since the comparison is made with a delayed version of the 256th count (see Fig. 9), this effectively advances the laser trigger with respect to the edge of the X-ray signal. This arrangement is used to compensate for the delay between the triggering of the laser and the occurrence of the actual light flash. In this way the actual laser flash is made to occur with $t_{delay} = (1 - N/256)\Gamma$.
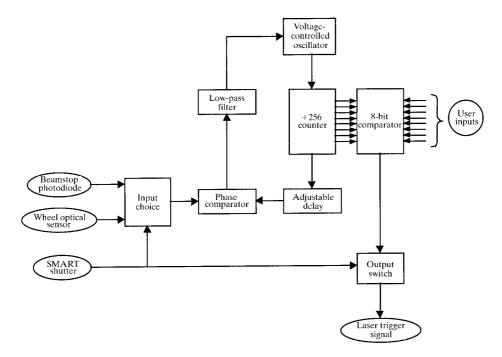

Figure 9
Schematic diagram of the circuit used to synchronize the X-ray and laser pulses. The trigger signal is generated either by the photodiode built into the beamstop or by an optical sensor mounted on the rotating shutter disk. Further details are given in the text.
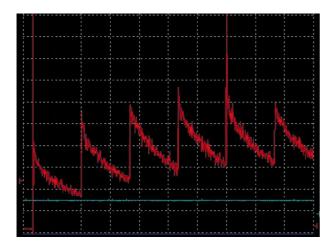
Figure 10
Fluorescence of a diffractometer-mounted sample of the dihydroxybenzophenone 18-crown-6 complex. One horizontal division corresponds to 20 ms. The effect of cumulative pumping is evident. The pseudo steady state is almost reached after the first six laser pulses shown here.

9. Concluding remarks

The system described above has been tested with a number of compounds, including a dihydroxybenzophenone-containing phase, specifically synthesized for time-resolved studies, in which the photoactive component is diluted with 18-crown-6 (Zhang *et al.*, 1999). The output of the photo-detector, obtained with a 80 Hz laser frequency (Γ = 12.5 ms), is reproduced in Fig. 10. The decay corresponds to a lifetime τ of 15–20 ms at the temperature of the experiment estimated at 30 K. The fluorescence trace shows the effect of cumulative pumping on the population of the excited species. The crystallographic analysis of the data will be reported in a separate publication.

Details of the configuration described above are subject to modification. We have, for example, made a different shutter wheel, and are considering other adjustments.

However, the instrumentation as described has performed well in a series of exploratory time-resolved experiments.

References

Bourgeois, D., Ursby, T., Wulff, M., Pradervand, C., Legrand, A., Schildkamp, W., Laboure, S., Srajer, V., Teng, T. Y., Roth, M. & Moffat, K. (1996). *J. Synchrotron Rad.* **3**, 65–74.
Coppens, P. (1997). *Synchrotron Rad. News* **10**, 26–30.
Coppens, P., Fomitchev, D. V., Carducci, M. D. & Culp, K. (1998). *J. Chem. Soc. Dalton Trans.* **6**, 865–872.
Fomitchev, D. V., Bagley, K. A. & Coppens, P. (2000). *J. Am. Chem. Soc.* **122**, 532–533.
Genick, U. K., Borgstahl, G. E. O., Ren, Z., Ng, K., Pradervand, C., Burke, P. M., Srajer, V., Teng, T. Y., Schildkamp, W., Mcree, D. E., Moffat, K. & Getzoff, E. D. (1997). *Science*, **275**, 1471–1475.
Moffat, K. (1998). *Acta Cryst.* A**54**, 833–841.
Ozawa, Y., Pressprich, M. R. & Coppens, P. (1998). *J. Appl. Cryst.* **31**, 128–135.
Ren, Z., Ng, K., Borgstahl, G. E. O., Getzoff, E. D. & Moffat, K. (1996). *J. Appl. Cryst.* **29**, 246–260.
Srajer, V., Teng, T. Y., Ursby, T., Pradervand, C., Ren, Z., Adachi, S., Schildkamp, W., Bourgeois, D., Wulff, M. & Moffat, K. (1996). *Science*, **274**, 1726–1729.
Tanimori, T., Ochi, A., Minami, S. & Naga, T. (1996). *Nucl. Instrum. Methods Phys. Res. A*, **381**, 280–228.
Uekusa, H., Ohashi, Y., Ochi, A. & Tanimori, T. (1999). XVIIIth IUCr Congress and General Assembly, Glasgow, UK, 4–13 August 1999. Abstracts, p. 236.
Zhang, Y., Wu, G., Wenner, B. R., Bright, F. V. & Coppens, P. (1999). *Crystal Eng.* **2**, 1–8.